Aerosol UV absorption experiment (2002-04): 2. Absorption optical thickness, refractive index and single scattering albedo

Nickolay Krotkov[*a], Pawan K. Bhartia[b] and Jay Herman[b], James Slusser[d],

Gwen Scott[d], Gordon Labow[c], Alexander P. Vasilkov[c],

Thomas F. Eck[a], Oleg Dubovik[a], and Brent N. Holben[b]

[a]Goddard Earth Sciences and Technology Center Univ. of Maryland Baltimore County, MD USA;

[b]NASA Goddard Space Flight Center, Greenbelt, MD USA;

[c]Science Systems and Applications, Inc., Lanham, MD USA 20706

[d]USDA UVB Monitoring Network and Colorado State University

[*] Krotkov@chescat.gsfc.nasa.gov; phone 1 301 614-5553; fax 1 301 614-5903; http://toms.gsfc.nasa.gov; GEST Center, NASA/GSFC Code 916 Greenbelt, Maryland 20771

ABSTRACT

Compared to the visible spectral region, very little is known about aerosol absorption in UV. Without such information it is impossible to quantify the causes of the observed discrepancy between modeled and measured UV irradiances and photolysis rates. We report results of a 17-month aerosol column absorption monitoring experiment conducted in Greenbelt, Maryland, where the imaginary part of effective refractive index, k, was inferred from the measurements of direct and diffuse atmospheric transmittances by a UV-Multifilter Rotating Shadowband radiometer (UV-MFRSR, USDA UVB Monitoring and Research Network). Co-located ancillary measurements of aerosol effective particle size distribution and refractive index in the visible wavelengths (by a CIMEL sun-sky radiometers, NASA AERONET network), column ozone, surface pressure and albedo constrained the forward radiative transfer model input, so that a unique solution for k was obtained independently in each UV-MFRSR spectral channel. Inferred values of *k* were systematically larger in the UV than in the visible wavelengths with largest k values at 325nm. The inferred k values allowed calculation of the single scattering albedo, ω, which was compared with AERONET inversions in the visible wavelengths. On cloud-free days with high aerosol loadings ($t_{ext}(440)$ >0.4), ω was systematically lower at 368nm ($<\omega_{368}>$=0.94) than at 440nm ($<\omega_{440}>$=0.96), however the mean ω differences (0.02) were within expected uncertainties of ω retrievals (~0.03). The inferred ω was even lower at shorter UV wavelengths ($<\omega_{325}>\sim<\omega_{332}>$=0.92), which might suggest the presence of selectively UV absorbing aerosols. It was also found that ω decreases with decrease in aerosol loading. This could be due to real changes in the average aerosol composition between summer and winter months at the GSFC site. Combing measurements of t_{ext} and ω, the seasonal dependence of the aerosol absorption optical thickness, $t_{abs}=t_{ext}\ (1-w)$ was derived in the UV with an uncertainty 0.01–0.02, limited by the accuracy of UV-MFRSR measurement and calibration. The t_{abs} had a pronounced seasonal dependence with maximum values ~0.1 occurring in summer hazy conditions and <0.02 in winter-fall seasons, when aerosol loadings are small. The measured t_{abs} was sufficient to explain both the magnitude and seasonal dependence of the bias in satellite estimates of surface UV irradiance previously seen with ground-based UV measurements.

Keywords: ultraviolet radiation, aerosol absorption, single scattering albedo, CIMEL sun photometer, AERONET network, UV multi-filter rotating shadow band radiometer, UV UV-MFRSR, diffuse fraction measurements

1. INTRODUCTION

Aerosols in the boundary layer can significantly change air quality either directly or by affecting the rate of tropospheric ozone (urban smog) formation[1-4]. Scattering by aerosols increases the actinic flux and the rates of photochemical reactions in the upper parts of the planetary boundary layer[1-6], while aerosol absorption reduces the amount of UV radiation available for chemical reactions within and below the aerosol layer[1-5]. Therefore, without accurate knowledge of aerosol UV absorption (or single scattering albedo) the magnitude and even the sign of the aerosol effect on tropospheric photochemistry remain highly uncertain[1-6]. By the same reasoning, the boundary layer aerosol absorption uncertainty remains a serious obstacle in satellite estimation of biologically harmful UV irradiance at the surface [7-13]. Although it is well known that iron oxides in desert dust[14-16] and soot produced by fossil fuel burning and urban transportation[17-21] strongly absorb UV radiation, properties of other potential UV absorbers, e.g., organic and nitrated and aromatic aerosols[22-23], are poorly known. In addition, different aerosol components are often mixed in an atmospheric column downwind from urban regions[24]. This makes it difficult to quantify aerosol effects on UV irradiance and photolysis rates from the models. On the other hand, ground based passive remote sensing techniques allow estimation of column aerosol absorption without prior knowledge of aerosol composition. The techniques are based on near simultaneous measurements of direct sun irradiance and diffuse sky radiance[25-28] or irradiance[29-34], from which column average absorption can be inferred (with aircraft measurements providing vertically resolved information[21,24]). The multi year mean column aerosol absorption climatology in the visible has been established for several sites using CIMEL almucantar inversions[25-27] from global AERONET network[35-36], but these inversions are not yet available at UV wavelengths. Ground-based remote measurements of aerosol UV absorption were also demonstrated[37-42], but these retrievals have not been validated. Neither technique has yet enabled deriving seasonal aerosol absorption climatology.

To validate column aerosol absorption retrievals in UV and produce a long-term seasonal data set of aerosol column absorption optical thickness, t_{abs}, a UV Multifilter Rotating Shadowband Radiometer (UV-MFRSR, Yankee Environmental Systems, Turners Falls, MA)[43-44] and a rotating triad of sun-sky CIMEL radiometers (reference instruments of NASA AERONET network[35-36]) were run side-by-side continuously for 17 months at NASA Goddard Space Flight Center in Greenbelt, Maryland. A previous paper[46] showed that the AERONET data could be used for UV-MFRSR daily on-site calibration and accurate measurements of t_{ext} at 3 UVA wavelength channels. The essential advantage of the schadowband technique[29-34] is that calibration obtained for direct-sun voltage can be directly applied to obtain diffuse atmospheric transmittance[43,46]. The transmittance combined with accurate t_{ext} data and a radiative transfer model allows the aerosol absorption and single scattering albedo retrievals described in this paper. The paper is organized as follows: section 2 describes briefly the data sets used in this study. Section 3 provides description of the UV-MFRSR inversion technique implementation and section 4 discusses aerosol absorption results and comparisons with AERONET inversion data in the visible wavelengths. Section 5 discusses application of the aerosol UV absorption optical thickness data to explain the bias in satellite surface UV estimates. Sensitivity study and accuracy assessments of the aerosol UV absorption retrievals are discussed in Appendix.

2. DATA SETS

The primary data set consists of 3–minute measurements of diffuse and total irradiance collected with the UV-MFRSR[43-44] instrument (optical head #271) from USDA UVB Monitoring and Research Network, UVMRP[45]. A single measurement cycle consisted of measuring total horizontal irradiance (no sun blocking) following by 3 irradiance measurements with different positions of the shadow band blocking the sun and sky radiance on each side of the sun (at 9^o). All spectral channels were measured within one second by 7 separate solid-state detectors with interference filters sharing a common Teflon diffuser[43]. The complete shadowing cycle takes ~10sec and was repeated every 3 minutes throughout the day without averaging of the data. The raw data (voltages) were automatically transmitted every night (via dedicated telephone modem) to the USDA UVMRP processing center at the Colorado State University (Fort Collins, CO) for voltage corrections and further processing. The standard UVMRP calibration procedure differs from that used in our experiments, where we used only cosine corrected voltages calibrated on-site against our co-located reference AERONET sunphotometers. This method yields more accurate measurements of $t_{\mathtt{ext}}$ and diffuse and direct atmospheric transmittances. Detailed description of the UV-MFRSR operating procedures, raw voltage corrections and on-site calibration procedure was a subject of the first paper (this issue)[46], therefore, only a brief summary is provided here.

2.1 Direct and diffuse transmittances

In addition to UV-MFRSR data, t_{ext} was continuously measured with rotating triad of CIMEL radiometers that were reference instruments of the AERONET global network (data available at http://aeronet.gsfc.nasa.gov)[35-36]. The automatic tracking Sun and sky scanning radiometers made direct Sun measurements with a 1.2^o full field of view every 15 minutes at 340, 380, 440, 500, 675, 870, 940, and 1020 nm (accuracy typically ~0.003 to 0.01 in the visible with larger errors in the UV[35,36,53]). The pressure corrected t_{ext} at 340nm, 380nm and standard t_{ext} at 440nm, 500nm were interpolated in time and wavelength and compared with the UV-MFRSR measurements of cosine corrected direct-normal voltages to derive a more accurate daily V_o calibration[46] than provided in the standard UVMRP data set (http://uvb.nrel.colostate.edu)[49]. The derived V_o for each spectral channel agreed with those from Langley UV-MFRSR measurements obtained on completely cloud-free days[46]. The improved calibration was used to obtain both direct (T_R) and diffuse (T_D) atmospheric transmittances with high accuracy (2%-4% at 368nm, see Table A1 in Appendix).

2.2 Surface pressure and total ozone measurements

Accurately specifying surface pressure is an important requirement for radiation modeling in the UV spectral region. Surface pressure measurements at nearby (5 km) USDA location in Beltsville, MD were used reduced by ~2mbar to account for change in altitude between Beltsville location (~70m asl) and GSFC UV-MFRSR location (roof of the building, ~90m asl according to our GPS measurements)[46].

Ancillary measurements at our site included Brewer double monochromator column ozone measurements. Missing Brewer ozone measurements were filled in with EP/TOMS total ozone data, since both ozone data sets agreed quite well (within 2%). The ozone values were used to calculate ozone absorption optical thickness, t_{O3} in each UV-MFRSR spectral channel for each individual measurement. The pressure measurements were used (1) to calculate accurate Rayleigh scattering optical thickness, t_R, and (2) to correct standard AERONET aerosol t_{ext} at 340nm, 380nm data used for calibration (see section 2.1).

2.3 Aerosol extinction optical thickness

Daily average V_o estimates along with t_R and t_{O3} were used to calculate aerosol t_{ext} for individual UV-MFRSR measurements[46]. The 3-minute UV-MFRSR t_{ext} data compared well with interpolated 15 minute AERONET t_{ext} measurements with only a small scatter (at 368nm daily rms differences between AERONET and UV-MFRSR t_{ext} were within 0.01 (1σ)) on all cloud-free days. This analysis[46] has shown that the UV-MFRSR, when inter-calibrated against an AERONET sunphotometer on the same day, was proven reliable to retrieve t_{ext}.

With t_{ext} known, the only RT model input parameters are surface albedo, A, aerosol phase function (average cosine, g) and single scattering albedo, ω. For ω to be inferred by means of fitting of calculated and measured transmittances, A and g were to be estimated from ancillary measurements as described below.

2.4 Aerosol phase function and asymmetry parameter

CIMEL sky radiance almucantar measurements at 440nm, 675nm, 870nm and 1020nm (downloaded from the web site: http://aeronet.gsfc.nasa.gov) were used in conjunction with t_{ext} at these wavelengths to retrieve column average particle size distribution, *PSD* and effective refractive index (real (n) and imaginary (k), independently at each of the above wavelengths) following methodology of Dubovik and King[25-27]. Even though it is well known that dust-like particles are irregular shapes arising from fracturing of larger grains, the AERONET retrieval assumes the aerosol particles to be polydisperse homogeneous spheres that have the same complex refractive index. Sensitivity studies by Dubovik et al.[26] examined how much these assumptions mislead the inversion solutions in the cases of nonspherical dust aerosols and in the case of non-homogenous aerosols (externally or internally mixed spherical particles with different refractive indices). For all tested cases no significant errors where observed in the retrieval of single scattering albedo, which is the focus of our study.

The aerosol phase function at UV-MFRSR wavelengths was calculated using AERONET *PSD* and refractive index at 440nm (real part) inversions within 60 minutes of each UV-MFRSR measurement using forward Mie calculations as described in section 3.

2.5 Surface albedo

It was previously shown that changes in A from 0.4 to 0.8 results in 30% increase in diffuse atmospheric transmittance[29-31]. However, in UV spectral region, A is only a few percent for snow-free terrain, therefore, climatological values are usually acceptable[54]. Excluding days with traces of partial snow cover allowed us to use Total Ozone Mapping Spectrometer (TOMS)-derived climatologically snow-free values of surface albedo [54]. Low surface albedo in UV A~0.02 at GSFC site was confirmed from satellite overpass 360nm reflectivity measurements from Earth Probe Total Ozone Mapping Spectrometer (EP/TOMS) on clear snow-free days (http://toms.gsfc.nasa.gov). Such low values of surface albedo provide an important advantage for measuring aerosol properties in UV spectral range. Maximum possible deviations ~0.02 in A from the assumed climatological value (A=0.02) would result in 1.5% changes in the diffuse irradiance transmittance and even smaller changes in total transmittance and diffuse fraction ratio.

2.6 Aerosol vertical distribution

The aerosol vertical distribution was shown to be not important for aerosol absorption determination (see later discussion in section 4). Therefore, a fixed exponential aerosol vertical profile in the lower troposphere was used in forward model with no stratospheric aerosol.

With t_{O3}, t_R, t_{ext}, A and g pre-determined in each UV-MFRSR channel, the only free RT model input parameter is single scattering albedo, ω. Therefore, ω was inferred with a forward radiative transfer model by requiring that calculated transmittances (or their ratio) match the measured ones (section 2.1) independently in each UV-MFRSR channel. Technically, Mie calculations were incorporated in the forward model to account for g spectral dependence without using look up tables. The details are given in section 3.

3. UV-MFRSR AEROSOL ABSORPTION INVERSION TECHNIQUE

Only UV-MFRSR data corresponding to horizontally homogeneous cloud-free atmospheric conditions were used. The cloud-free portions of days were selected by visual examination and analysis of 3-minute irradiance series and all-sky camera images.

The fitting to the forward model was done separately for different transmittances and their ratios (the diffuse to direct ratio ($D_D=T_D/T_R$)[29-31], diffuse fraction ($D_T=T_D/T_T$)[32-34] and the total transmittance ($T=V_T/V_0$)[7]) at each UV-MFRSR spectral channels. The advantage of utilizing dimensionless ratios (D_D, D_T and T) is that absolute radiometric calibration is not needed, since the same detector measures both the total and diffuse flux[43]. Agreement between all 3 methods provides a robust check on relative UV-MFRSR spectral calibration and correction for systematic measurement errors (i.e. angular and spectral response corrections)[46].

To obtain the UV-MFRSR aerosol inversions, CIMEL almucantar inversions[25-27] were used (section 2.4) obtained in a 5 minute interval approximately once per hour and direct-sun τ_{ext} obtained every 15 minutes (section 2.3). All available UV-MFRSR data (every 3 minutes) within time interval ±60min of each AERONET almucantar measurement were analyzed. Our assumption was that the aerosol type did not change during this period and that observed changes in the radiation field arise from changes in solar zenith angle and aerosol optical thickness. Therefore, we used the same aerosol size distribution and real part of refractive index within each 60-minute time slot, but allowed for t_{ext} and q_0 changes in 3-minute increments using UV-MFRSR measurements. If timeslots for 2 consecutive AERONET retrievals overlap, we repeated the UV-MFRSR fitting for all overlapping points with the new aerosol parameters. This provided a test of sensitivity of our results to real-time changes in the AERONET inversion parameters (PSD and n_R) used as input to our fitting technique. Forward RT calculations were run to fit every single 3-minute UV-MFRSR measurement independently at each wavelength. The advantage of this approach is that forward RT calculations were always done for the exact values of solar zenith angle, t_{ext}, and aerosol parameters. The methodology of forward modeling and ω retrieval was as follows:

1) Standard discrete AERONET column volume *PSD* in 22 size bins between 0.05μm and 15μm were fit using a bi-modal lognormal volume size distribution[27]. This parameterization requires 6 input parameters: column volume, modal radius and standard deviation separately for fine and coarse modes.
2) Volume PSD parameters were analytically converted to column number density parameters required as input to the Mie code[55]. Since only the shape of the PSD was required, five input parameters remained: modal radii and standard deviations separately for fine and coarse modes and the ratio of the total number of particles in fine and course modes. The implicit *PSD* normalization occurs by requiring the model input t_{ext} equal to UV-MFRSR measured t_{ext}.
3) In our Mie code the refractive index was assumed to be the equal for fine and coarse modes (one component aerosol model) to be consistent with AERONET inversions[25-27]. Thus, following current AERONET assumptions, a single optically effective refractive index was retrieved, which was a weighted mean of the true column average refractive index over particle size distribution.
4) The real part of refractive index, n, was assumed to be constant with wavelength, and was fixed to the AERONET retrieved value at 440nm. This approximation was possible, since the direct transmittance was forced to be equal to the measured one through the independently measured t_{ext}, while diffuse irradiance only weakly depends on the real part of refractive index[29-31].
5) An a-priori vertical profile shape of the aerosol loading was assumed in our forward model that peaks in the boundary layer. The additional assumption was that neither aerosol PSD nor the refractive index change with altitude, which was consistent with AERONET inversions[25-27]. No stratospheric aerosol was assumed.

6) In the forward RT model, the TOMS climatological ozone and temperature profiles were used that were scaled to the Brewer measured total column ozone amount for every actual UV-MFRSR measurement. The Brewer total ozone amount compared well with TOMS

ozone measurements so that TOMS ozone values could be used to fill in days with missing Brewer ozone measurements. No gaseous absorption other than ozone was assumed.

7) The ancillary measurements available at GSFC location (see section 2) allowed us to constrain all required input to the Mie scattering code within the forward RT model, except the imaginary part of the aerosol refractive index, k, which is related to effective column aerosol absorption. The k was inferred by fitting either diffuse to direct ($DD=V_F/V_D$) or diffuse fraction ($D_T=V_F/V_T$) or total transmittance ($T=V_T/V_0$) measurements to the RT calculated values separately in each spectral channel. The fitting was done iteratively starting with AERONET derived k_{440} as the initial value. The absolute value of the fitting residual was used as a measure of the goodness of the fit.

8) If a good fit was achieved, the *k(fit)* was treated as an optically effective fitting parameter, rather than microphysical particle property, because it accounts for all assumptions in the forward model as well as systematic measurement errors. The fitted value of *k(fit)*, along with the AERONET *PSD* and n_{440}, were used to calculate single scattering albedo, *w(fit)*, using Lorentz-Mie code and $t_{abs}=(1-w(fit))t_{ext}$. Derived radiative properties (w, t_{abs}) were less dependent on model assumptions so that their errors were smaller than errors in k (see Appendix for estimation of errors).

9) As an independent check, the diffuse fraction we estimated varying w directly as input parameter to a different RT code (TUV4[6] based on the DISORT[56] radiative transfer code). Both w retrievals agreed well (within 0.01) at 368nm provided that the CIMEL derived value of the asymmetry parameter, g_{368}, was used as input to the TUV model. This check provides confidence that Mie model assumptions and forward RT calculations were not a major source of error in the retrievals of ω and t_{abs}.

4. UV-MFRSR RETRIEVAL RESULTS

The inferred values of k and ω in the UV wavelengths were used (1) to compare with independent AERONET ω (section 4.1) and k (section 4.2) retrievals at 440nm and (2) to infer seasonal dependence of aerosol absorption optical thickness, $t_{abs}=t_{ext}(1-\omega)$ (section 4.3). The comparison dataset was limited because of the following requirements. Completely cloud-free periods were manually selected (using visual sky observations), coincided with UV-MFRSR calibration periods [46]. Days with partial snow cover were manually filtered out, with ~100 cloud-free portions of days remained between October 1, 2002 and March 25, 2004, meeting our cloud-free and snow- free criteria. To compare only high quality w and k retrievals only the inversions with $t_{ext}(440nm)>0.4$ and solar zenith angle, $\theta_o>45^o$ (required for good AERONET inversions[25-27]) and $\theta_o<70^o$ (required for good UV-MFRSR inversions to minimize cosine correction errors[46]) were selected.

For all cases UV-MFRSR data were processed 3 times using different measured fitting parameters (diffuse/direct voltage ratio, diffuse/total voltage ratio and total normalized transmittance V_T/V_0). All 3 methods provided consistent inversion results (within 0.01 in ω). As an additional check, the comparisons were made with *w* retrievals not using a different forward RT code (TUV[6]). The retrievals were essentially the same (ω within 0.01) when the correct g factor was used in the forward model (TUV[6]). Selected ω comparison cases are shown in Figures 1-3.

4.1 Single scattering albedo

Figure 1 shows *w* retrievals by both instruments on June 2 2003, when a long-range smoke plume was moving over GSFC location. The passage of the plume was evident from enhanced extinction optical thickness, t_{368}, measured by both instruments (shown on the right axis in figure 2). Visually, horizontal visibility remained high on this day with clear sight of horizon; however, the sky color was unusually white. According to the 3-min UV-MFRSR data, the most absorbing part of the smoke plume (ω_{368} ~0.88-0.9) was recorded in the morning (<14UT) with less absorbing w_{368} ~0.93 for the rest of the day. Back trajectory analysis and satellite data suggested that the smoke plume was originated from fires in Siberia near lake Baikal. Physical-chemical processes during long-range transport of smoke can explain this relatively low absorption. Boreal forest smoke typically does not have low *w* due to significant particle production from smoldering of woody fuels, which yields relatively small black carbon percentages. Also smoke particles tend to become less absorbing with age as the particle size increases due to coagulation during transport[57]. The Angstrom exponent was high and stable during the day ($\alpha_{440/870}$=1.73-1.88), suggesting predominantly fine-mode particles. However, the Angstrom exponent was smaller in UV ($\alpha_{380/440}$=0.73-0.82) compared to the visible wavelengths. This suggests substantial curvature of the ln(τ) vs ln(λ) dependence (α'=1.7-1.8)[24,29]. The cause of large ω discrepancy in the morning (~11.5UT) remains unknown.

Although complete AERONET inversions were available for the whole day, w_{440} retrievals were not shown for solar zenith angles less than 45°, because the uncertainty in w_{440} is significantly larger for these cases[26,27]. However, AERONET inverted particle size distribution results were shown to be accurate for all conditions[26,27] and they are used for UV-MFRSR retrievals without restriction on solar elevation. On the other hand, UV-MFRSR ω_{368} retrievals were not shown for high solar zenith angle cases when q_o>75°, because the cosine-correction uncertainty for the measured diffuse irradiance is larger for these cases[46]. The additional uncertainty at high solar zenith angles arises from using a pseudo-spherical version of the forward radiative transfer code, which corrects only direct sun irradiance, thus underestimating diffuse irradiance[55]. Thus, the two methods of estimating ω are complementary in that the AERONET[25-27] retrieval requires large solar angles, while UV-MFRSR data are more reliable at low solar zenith angles.

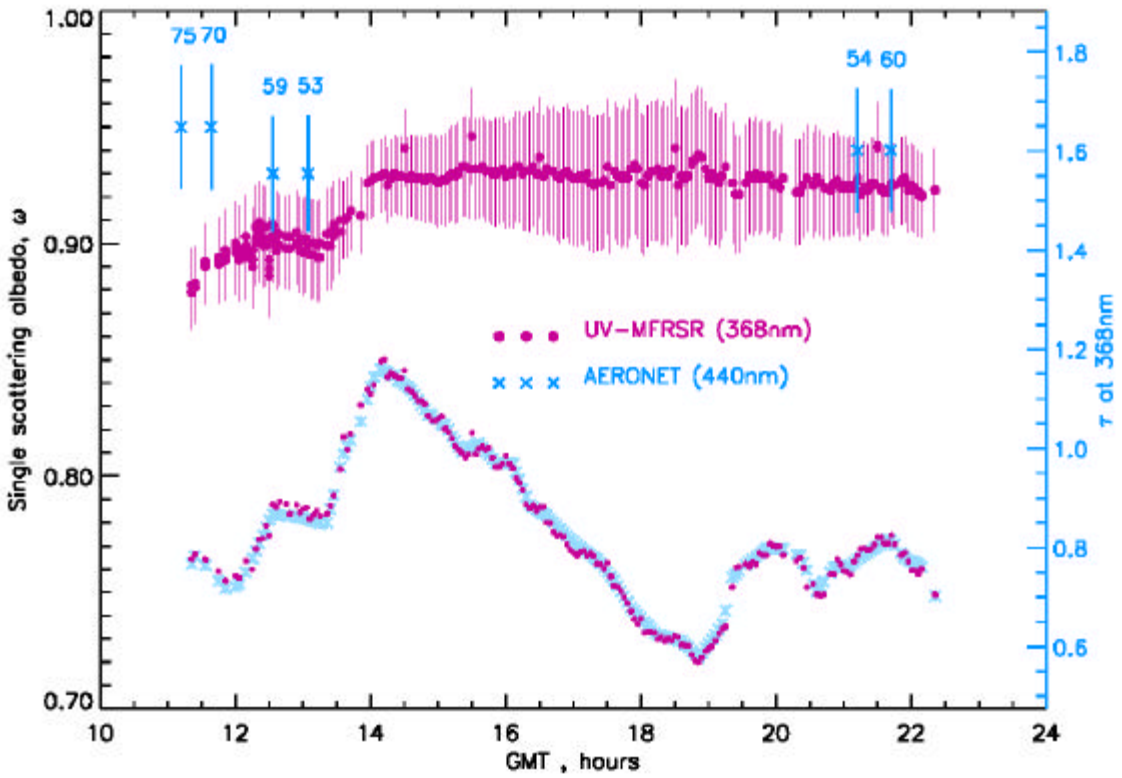

Figure 1 *UV-MFRSR and AERONET single scattering albedo retrieval at GSFC on June 2 2003. The 3-minute UV-MFRSR retrieved w at 368nm are shown as small purple spheres, while AERONET w* $_{440}$ *retrievals at 440nm are shown as large crosses with +/- 0.03 error bars*[26]*. In addition,* t_{ext} *at 368nm is shown for both instruments (same symbols) with right axis scale. The actual solar zenith angle was used in retrieval for each 3-min UV-MFRSR measurement. The UV-MFRSR assumptions were: surface albedo 0.02, Brewer measured total ozone, boundary layer aerosol profile and AERONET* [25]*inverted particle size distribution within ± 60min of each CIMEL almucantar measurement.*

The real part of refractive index at 440nm, n_{440}, increased from 1.39 to 1.5 during smoke passage and decreased later to 1.46. The imaginary part of refractive index was systematically higher in UV than in the visible (k_{368}=0.014 - 0.02, k_{440}=0.007 – 0.013). The difference was larger than specified uncertainty for AERONET k retrievals (±0.003)[27] for all cases except one retrieval. These differences in k were consistent with lower ω values in UV (ω_{368}=0.89-0.92 compare to ω_{440}=0.93-0.95). This suggests that ω spectral dependence in the visible (lower ω at longer wavelengths)[27] flattens out and even reverses in UV. However, it is emphasized that, except for solar zenith angles larger than 70^o , the ω retrieved at 368nm and 440nm are within the range of overlap of both retrieval uncertainties.

The sensitivity of ω_{368} results to assumed aerosol vertical profile was also studied. The smoke plume height over Eastern Shore in Maryland and Virginia was ~3km according to Lidar data

(UMBC elastic lidar system (ELF) at Chesapeake Lighhouse, 36°54.6'N, 75°42.6' W). Therefore, UV-MFRSR retrievals were repeated with aerosol height at 3km with essentially unchanged ω results. Therefore it was concluded that UV-MFRSR results were not sensitive to the smoke vertical profile (at least at 368nm).

Figure 2 shows ω comparisons on June 24 2003, which was typical for a summer local ozone pollution episode. A high-pressure system over the Mid-Atlantic region for this week prevented air exchange; therefore tropospheric ozone pollution was building up as a result of local pollution (mostly traffic) and high solar irradaince[5] (air quality public warning was "Code orange" on this day). The conditions were mostly cloud-free for the whole day. In the morning aerosol absorption was higher in UV, but differences were not significant. Aerosol extinction decreased during the day, while absorption increased slightly, but more rapidly in the visible. In the afternoon both ω retrievals were in agreement (ω_{368}=0.91-0.92, ω_{440}=0.91-0.92). AERONET inverted real part of refractive index at 440nm was changing changed between 1.39 and 1.59. The Angstrom exponent was much higher than for smoke event on June 2, especially in UV due to significantly smaller radius and broader σ of the fine mode on June 24.

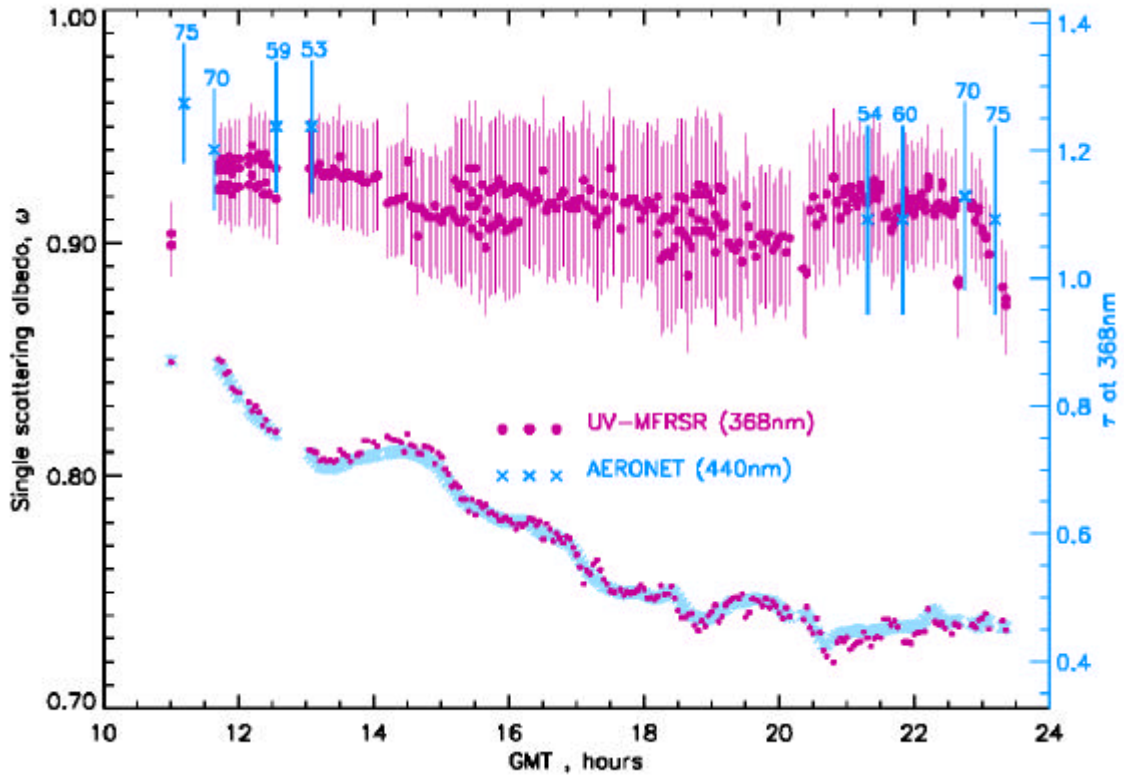

Figure 2 *UV-MFRSR and AERONET w retrieval at GSFC on June 24, 2003. The 3-minute UV-MFRSR* w_{368} *is shown as small purple spheres, while AERONET* w_{440} *retrievals are shown as large crosses with ±0.03 error bars*[27]*. In addition,* t_{ext} *at 368nm is shown for both instruments (same symbols) with right axis scale. The actual solar zenith angle was used in retrieval for each 3-min UV-MFRSR measurement. The UV-MFRSR assumptions were: A= 0.02, Brewer measured total ozone, boundary layer aerosol profile and AERONET* [25]*inverted particle size distribution within ±60min of each CIMEL almucantar measurement.*

Strong daily variation in w_{368} was detected on August 25, 2003 (**Figure 3**) with unusually low values (w_{368} ~0.85) in the middle of the day. This case highlights the importance of measuring the complete diurnal cycle of summertime aerosol absorption, not just morning and afternoon periods.

This case also illustrates the sensitivity of UV-MFRSR retrievals to the real part of refractive index. As was mentioned in section 3, AERONET inversions of PSD and refractive index (real part at 440nm, n440) within 60 minutes of the individual UV-MFRSR measurement were used as input to the UV-MFRSR forward RT model. If the timeslots for 2 consecutive AERONET retrievals overlap, as in case of UV-MFRSR retrievals between 20.67UT and 21.2UT, the UV-MFRSR inversions were repeated for all overlapping points with the new set of AERONET input aerosol parameters (i.e using 21UT retrieval in Figure 3). In this particular example, *PSD's* were close for 2 consecutive AERONET retrievals ($R_{V,fine}$=0.14μm, $ln(s_{fine})$=0.38 at ~20.67UT versus R_{Vfine}=0.15μm, $ln(s_{fine})$=0.38 at ~21.2UT), but n_{440} increased significantly (from 1.33 to 1.56), causing g_{368} to decrease for the latter AERONET retrieval (g_{368}=0.735 using n_{440}=1.33 at ~20.5UT and g_{368}=0.676 using n_{440} =1.56 at ~21UT).

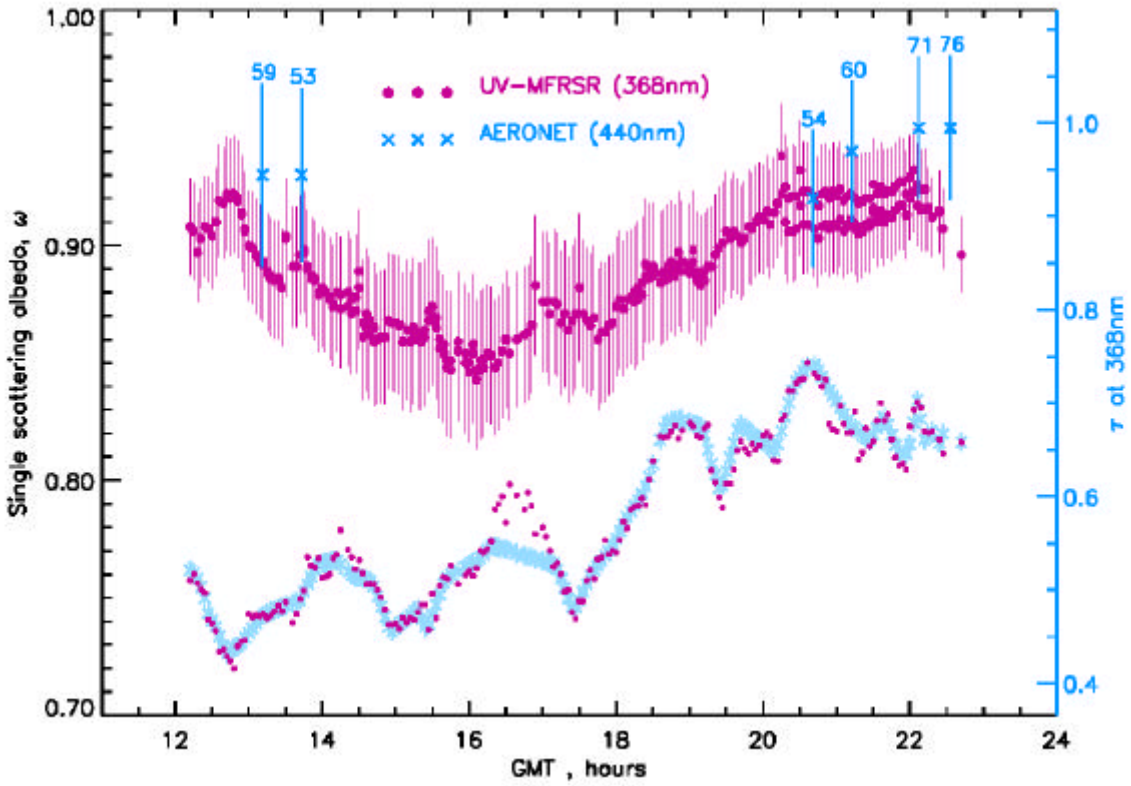

Figure 3 *UV-MFRSR and AERONET w retrieval at GSFC on August 25, 2003. The 3-minute UV-MFRSR w_{368} is shown as small purple spheres, while AERONET w $_{440}$ retrievals are shown as large crosses with ±0.03 error bars*[27]*. In addition, t_{ext} at 368nm is shown for both instruments (same symbols) with right axis scale. The actual solar zenith angle was used in retrieval for each 3-min UV-MFRSR measurement. The UV-MFRSR assumptions were: surface albedo 0.02, Brewer measured total ozone, boundary layer aerosol profile and AERONET* [25]*inverted particle size distribution within ±60min of each CIMEL almucantar measurement.*

The effect of changing g on fitted w can be understood using a two-stream approximation[58]:

$$T_T(calc) \cong 1 - \frac{(1-g_{368})t_{ext}}{(1-g_{368})t_{ext} + 2m_o} \qquad (1)$$

According to the equation (1) the decrease in g_{368} (meaning less asymmetric phase function) would cause calculated $T_T(calc)$ to decrease with fixed t_{ext} and solar zenith angle ($m_o=cos(q_o)$~0.5) (see also similar calculation in[30]). Therefore, fitting the measured $T_T(meas)$ with this new $T_T(calc)$ would require less absorption or larger inverted w_{368}. The actual w_{368} retrievals (figure 3) show that increase in input $n_{440}(=n_{368})$ does cause the increase in inverted w_{368} in agreement with our estimate. Less pronounced jumps in w_{368} retrievals caused by changing in AERONET input parameters can be seen on other retrieval days and times (figures 1-3). However, the jumps were typically within the range of overlap of w retrieval uncertainty, and were considered insignificant.

Table 1 provides ω comparison statistics on days with high aerosol loadings ($t_{ext}(440)$ >0.4), (60 matchups mostly in Summer 2003), when both retrievals were most accurate. It was found that on average ω was lower at 368nm ($<\omega_{368}>$=0.94) than at 440nm ($<\omega_{440}>$=0.96). However, the mean ω differences (0.02) were within uncertainties of UV-MFRSR retrievals (~0.03, see Appendix). It should be also mentioned that for AERONET wavelengths, ω increases with decreasing l in the visible for fine mode smoke or pollution aerosol[27]. Therefore, the extrapolated differences in w_{368} (predicted by AERONET) and w_{368} retrieved by UV-MFRSR may be slightly greater than direct comparisons of w_{440} to w_{368}. The inferred ω was even lower at shorter UV wavelengths ($<\omega_{325}>$~$<\omega_{332}>$=0.92) that might suggest the presence of selectively UV absorbing aerosols or gases other than ozone. The spectral differences between 325nm and 332nm were statistically insignificant, which could be explained by small separation in wavelength (7nm) between these 2 channels. All ω spectral retrievals were highly correlated for either UV-MFRSR or AERONET inversions (correlation coefficient >0.9, Table 1). However, the correlation was weaker between UV-MFRSR and AERONET wavelengths.

The average AERONET ω retrievals for summer 2003 ($<\omega_{440}>$=0.96) were lower than multiyear average at the same site ($<\omega_{440}>$=0.98)[27] suggesting unusually high absorption. This difference could be a result of a statistical fluctuation (our sample includes only 60 cases, while much larger sample was used in [27]) or could reflect real interannual changes in aerosol absorption. Since the ω retrievals were correlated in the UV and visible wavelengths (correlation coefficient ~0.6-0.7) this could also mean that the true (multiyear) climatological absorption in UV wavelengths is, perhaps, higher by ~0.02 than 2003 summer mean value ($<\omega_{368}>$=0.94, Table 1). Continuation of the long-term continuous measurements by both techniques is therefore important to increase statistical significance of our results.

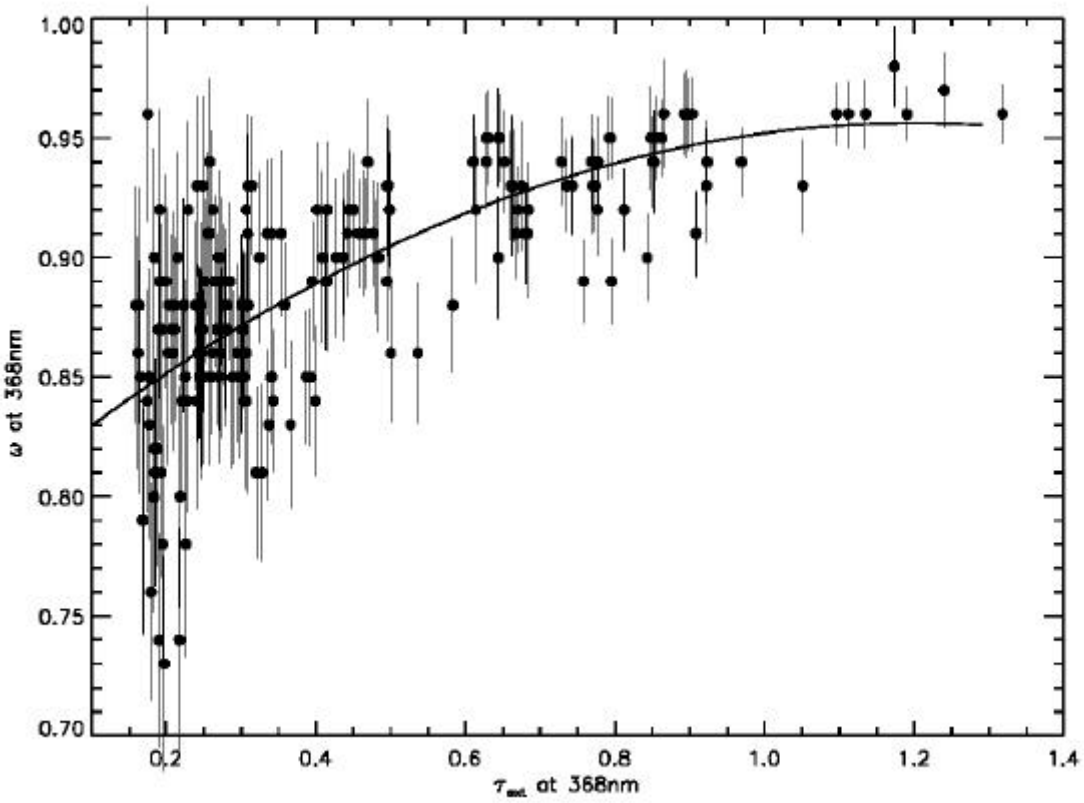

Figure 4. 2-hour average retrieved values <w_{368}> as function of measured extinction optical thickness, t_{abs} at 368nm for 17 months UV-MFRSR operation at NASA GSFC site. The error bars are interpolated from Table A1 (Appendix) and are assumed the same as for individual retrievals. The error bars were not reduced, despite 2 hour averaging of individual retrievals, because retrieval errors were not believed to be random. Only <w_{368} > values with estimated retrieval uncertainties less than 0.05 are shown.

The results in Table 1 were obtained under conditions of high aerosol loadings (t_{ext} *(440) > 0.4*) that were mostly restricted to summer humid haze conditions. The aerosol loadings are typically much lower at GSFC site in Fall-Winter-Spring seasons. The key question is whether the aerosol absorption remains seasonally independent and whether the *w* results obtained during summer conditions (Table 1) could be used for other seasons? To investigate this question the UV-MFRSR *w* retrievals were repeated allowing cases with lower aerosol loadings (t_{ext} *(440) > 0.1*) and correlated versus t_{ext} . The largest correlation between *w* and t_{ext} (with correlation coefficient ~0.7) was found at 368nm (Figure 4), while correlation was weaker at other wavelengths (~0.6 at 325nm and ~0.4 at 440nm and 670nm). The decrease of ω with t_{ext} suggests that the type of aerosol may have changed between summer and winter conditions. It is well known that aerosols in the mid-Atlantic region in summer are strongly hydroscopic[57], therefore particle growth by swelling at high relative humidity may be partly the reason for reduced absorption in summer[27].

Indeed, annual cycle of w_{368} is the same as t_{ext} annual cycle: with maximum in summer and minimum in winter. Limited number of previous ω retrievals in UV revealed larger variability of ω at different locations[7,24,37-42]. For example, w retrievals using all channels of UV-MFRSR were conducted at Black Mountain, NC[38,40-41]. The authors report w_{368} ranging from 0.81 to 0.99 with the average value $<w_{368}>$=0.89 and estimated uncertainty ±0.04 at t_{ext}~1. On the other hand, estimates of w_{325} in Toronto, Canada, using total (global) irradiance measured with Brewer spectrophotometer (w_{325} ~0.95 see Table 1 and figure 12 from Krotkov et al[7]) were only insignificantly higher than current UV-MFRSR summer average value $<w_{368}>$=0.94 at GSFC location.

4.2 Imaginary part of refractive index

Incorporating aerosol Mie calculations along with AERONET inversions of the particle size distributions and real part of refractive index into the RT forward model made it possible to infer optically effective imaginary part of refractive index, k independently in each UV-MFRSR spectral channel (for details see section 3). The combined statistics of UV-MFRSR and AERONET spectral k retrievals on hazy summer days (t_{ext} *(440) > 0.4*) is presented in Table 2. The retrieved k values were higher in UV than in the visible wavelengths: $<k_{368}>$~0.009±0.004 compare to $<k_{440}>$~0.006±0.003. However, mean differences in k ($<k_{368}-k_{440}>$~0.004, $\sigma_{k368-k440}$~0.003) were only slightly larger than AERONET quoted retrieval uncertainty Dk~0.003[27]. The k values were even higher at shorter UV wavelengths: $<k_{325}>$~0.013±0.005. Therefore, k spectral dependence in the UV was found to be similar to the spectral absorption of organic carbon (OC) from biomass burning (Table 4, reference[23]), while AERONET k retrievals were more consistent with the assumption that Black carbon (BC, from urban and motor vehicle emissions[23]) was the main absorber in the visible wavelengths[27]. These apparent differences need further investigation.

So far, UV-MFRSR w and k results (Tables 1 and 2) do not allow explanation of the causes of apparent larger absorption in the UV wavelengths compare to AERONET retrievals in the visible wavelengths. This could be due to differences in the techniques or the presence of selectively absorbing aerosols in the UV and needs further study. Enhancing both techniques to provide a spectral overlap with at least one common wavelength would provide better insight on aerosol absorption spectral dependence. At the same time conducting co-located measurements at different sites with varying background aerosol conditions is also desirable.

4.3 Aerosol absorption optical thickness

Ultimately, our goal with UV-MFRSR measurements was to derive statistical distribution (daily and seasonal) of the UV absorption optical depth, t_{abs} at urbanized region in the Eastern part of the US[5]. The $t_{abs}=t_{ext}(1- w)$ can be calculated using UV-MFRSR t_{ext} and w inversions or directly using linear regressions (see Figure A1 in Appendix). It should be noted that using regressions to

estimate t_{abs} directly from irradiance measurements allows retrievals under smaller aerosol loadings than typically assumed in retrievals aerosol absorption. Additional advantage is that t_{ext} is typically 50% -100% larger in the UV than in the visible wavelengths for urban-industrial aerosol with the same mass loading. These conditions make it possible to estimate t_{abs} for smaller aerosol loadings ($t_{abs}(440)>0.1$), which in turn allowed, for the first time, studying the seasonal cycle in aerosol absorption. Figure 5 shows timeseries of hourly $<t_{abs}(368)>$ values for 17 months continuous monitoring at GSFC site (cloud free and snow-free cases).

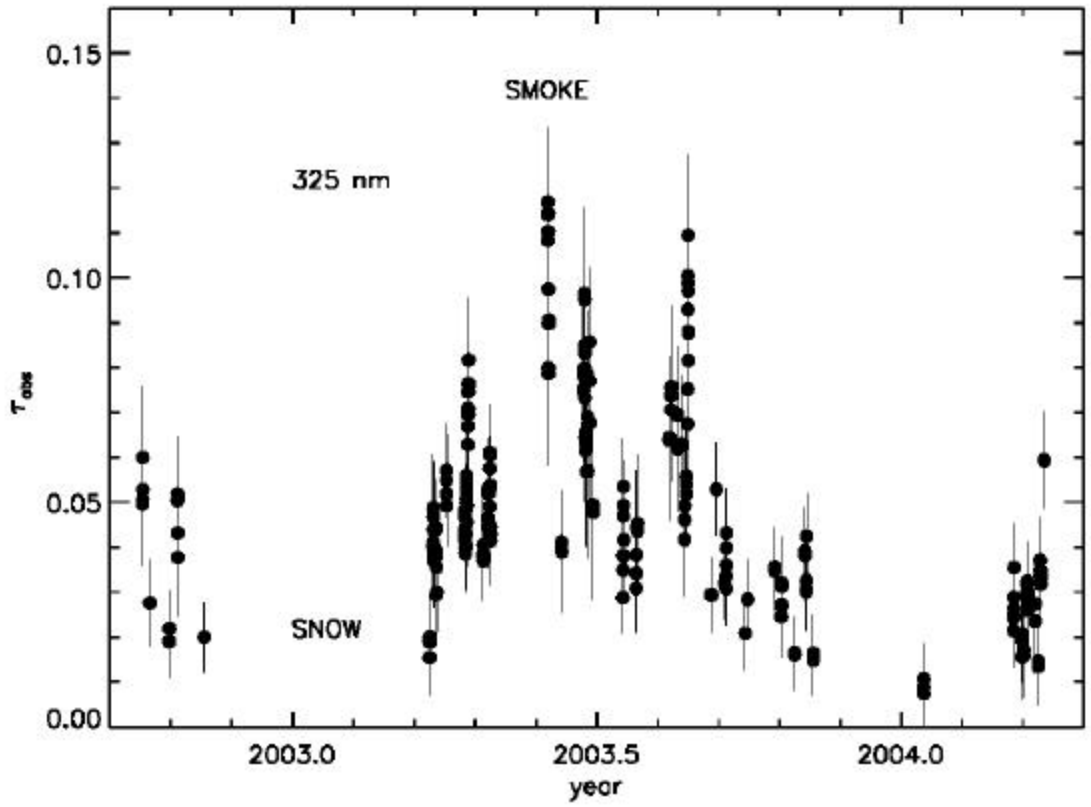

Figure 5. Timeseries of aerosol absorption optical thickness t_{abs} at 368nm, derived from 17 months UV-MFRSR operation at NASA GSFC site in Maryland, US. The data are for cloud-free and snow free conditions and $t_{abs}(440)>0.1$. Individual $t_{abs}(368)$ values were averaged over 1-hour period of time within ±60min of the AERONET inversion. The error bars of $t_{abs}(368)$ are interpolated by $t_{abs}(368)$ and solar zenith angle from estimates given in Appendix Table A1.

The data gaps occurred due to unusually unfavorable weather conditions (rain or snow) in 2003 or from exceptionally clear days with $=t_{ext}(440)<0.1$. Still main features of the t_{abs} seasonal cycle at GSFC can be clearly seen from the figure: a pronounced summertime maximum with

$t_{abs}(368)$~0.06-0.07 and wintertime minimum ~0.01. The maximum t_{abs} typically occurs in summer due to combination of regional and local pollution sources with hot and humid weather conditions (summer haze). The weakly absorbing haze (ω_{368}>0.94) is often associated with and enhances high levels of tropospheric ozone (ozone smog episodes)[5]. These summer haze conditions are responsible for summer high t_{abs} values (at *368nm* ~0.06-0.07). Even on relatively clear summer days t_{abs} is larger than ~0.02. On top of the seasonal cycle, occasional transient phenomena (long-range transport of biomass burning smoke and desert dust storms) can be clearly detected. One clear example was the passage of an aged smoke plume from Siberian forest fires over GSFC on June 2, 2003 (Figure 1), characterized by an unusually large $t_{abs}(368)$~0.085. Although occasional dust plumes had been reported at GSFC (for example, April 2001 Asian dust plume), no dust events occurred during reported time period.

While the annual cycle in t_{abs} is caused mainly by the annual cycle in aerosol extinction optical thickness, t_{ext}, the correlation between t_{abs} and t_{ext} was not perfect (linear correlation coefficient ~0.76 at 368nm), as would have been the case with no variability in aerosol single scattering albedo, w=*const.* Indeed, w_{368} data presented in Figure 4 (as well as at other wavelengths) might suggest that w is, indeed, not constant, but decreases with decreasing t_{ext}. The downward w trend was seen for both UV-MFRSR and AERONET inversions, despite progressively larger retrieval errors at small t_{ext}. This trend could be due to real changes in the average aerosol composition between summer and winter months at the GSFC site.

5. Explaining bias in satellite UV irradiance retrievals

Aerosol UV absorption results reported here have important implications for measuring UV surface irradiance from space. Multiyear comparisons of the TOMS UV data with ground-based Brewer measurements revealed a positive bias at many locations[7-10]. The bias can be seen at all wavelengths in clear-sky conditions. This suggests the difference is not related to ozone absorption. Here we estimate possible bias explanation due to aerosol absorption effects[10,59]. The TOMS UV algorithm first involves estimation of a clear-sky surface irradiance, E_{clear}, which is adjusted to actual surface irradiance, E, by using a TOMS-derived cloud/aerosol transmittance factor, C_T :

$$E = E_{clear} C_T \qquad (2)$$

Either cloud or absorbing aerosol index (*AI*) correction is applied to calculate C_T[7-10]. Currently absorbing aerosols are assumed and *AI* correction is applied if *AI*>0.5 and 360nm reflectivity <0.15. Otherwise, cloud C_T model is assumed, so the algorithm does not distinguish between thin clouds and aerosols. This causes a typical C_T error ~2% for non-absorbing sulfate or sea salt aerosols with t_{ext}(550)=0.2. On the other hand, absorbing aerosols in the boundary layer attenuate UV irradiance more strongly for the same t_{ext}, causing cloud C_T correction to underestimate their attenuation of surface UV irradiance. Because pollution aerosols are typically located in the boundary layer, they tend to produce negative AI that makes it impossible to distinguish from non-

absorbing aerosols and thin clouds using just AI data causing overestimation of UV irradiance. Moreover, since these aerosols also attenuate the outgoing radiation, the cloud C_T algorithm underestimates t_{ext}, amplifying the error further. The TOMS UV bias was modeled and shown to be proportional to t_{abs}.[10, 59] Here we quantified the bias using actual TOMS and UV-MFRSR measurements combined with retrievals of the aerosol optical properties as follows:

1) Top of the atmosphere radiances were measured by TOMS at 331nm and 360nm and inverted with a standard TOMS surface UV algorithm[10] to obtain estimates of surface UV irradiance at 325nm, UV(TOMS);
2) TOMS absorbing aerosol index, AI, was also calculated to select conditions with no free-troposphere absorbing aerosol plumes: AI < 0.5.
3) UV(TOMS) was compared with the UV-MFRSR measured total UV irradiance to estimate the bias: UV(TOMS)/ UV(ground);
4) The bias was correlated with UV-MFRSR measurements of $t_{abs}(325nm)$ (Figure 6).

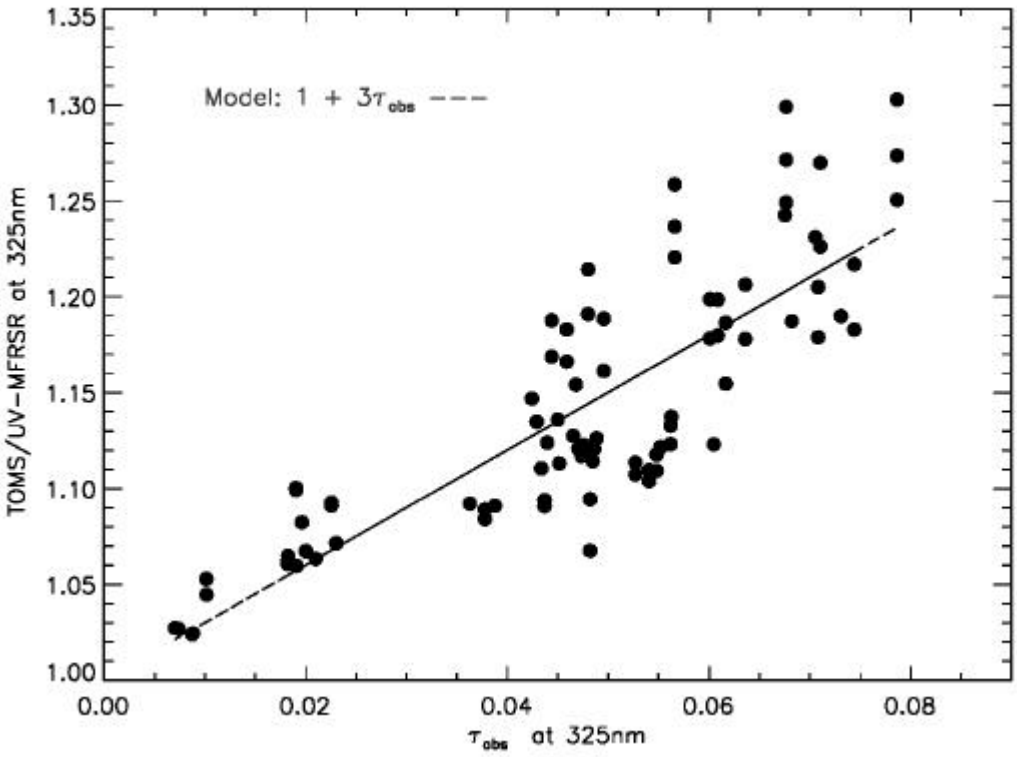

Figure 6 The ratio between satellite estimated (by TOMS UV algorithm[7-10]) and measured (by UV-MFRSR) total (direct plus diffuse) surface UV irradiance at 325nm versus aerosol absorption optical thickness at 325nm inferred from combined UV-MFRSR and AERONET measurements at NASA GSFC site. The line shows theoretical relationship derived from radiative transfer modeling[10]. The results are shown only for pollution aerosols with TOMS absorbing aerosol index, AI at 331nm less than 0.5 and TOMS 360nm Lambertian effective reflectivity

Figure 6 shows that the bias was indeed well correlated with $t_{abs}(325nm)$ and, the slope of the regression was close to theoretically predicted parameterization. This confirms that boundary layer aerosol absorption can indeed explain the positive TOMS UV bias found in ground-based land comparisons. Since operational global satellite UV algorithm was not expected to catch all variability in local atmospheric and geographical conditions at measurement sites, the bias was parameterized as function of t_{abs} to provide off-line correction for the operational UV(TOMS) data, so users at sites with t_{abs} ground measurements or established climatology can apply their own corrections to the standard TOMS UV data off-line.

$$UV(corrected) = \frac{UV(TOMS)}{1 + 3t_{abs}(l)} \qquad (3)$$

6. CONCLUSIONS

1) It was demonstrated that an advantage of the shadowband technique in measuring aerosol absorption is that the accurate irradiance calibration can be established by calibrating the direct sun component and comparing with sun-photometers such as AERONET CIMELs. The shadowband method is complementary to the AERONET almucantar retrieval of aerosol single scattering albedo[25-27], because the retrievals are more reliable at low solar zenith angles. Therefore, combined use of both instruments allows deriving the complete diurnal cycle of aerosol absorption.

2) There are specific advantages in measuring aerosol absorption in UV that let us to believe that *w* retrieval results can be used down to t_{ext}*~0.2*: (1) the measured accuracy of AERONET reference instruments in the UV with additional pressure and true ozone corrections could be made perhaps better than the previously estimated value of ~0.01 at 340nm [35-36,53]; (2) the surface albedo is much smaller in UV than in the visible spectral region and does not affect as much the aerosol retrievals; (3) t_{ext} is larger (for the same aerosol mass) than in the visible spectral range; (4) careful characterization of UV-MFRSR instrument, correction for known systematic errors, monitoring of instrument performance via daily CIMEL intercomparisons and characterizing atmospheric conditions; (5) stability and repeatability of individual *w* retrievals; (6) ancillary and redundant aerosol measurements available at GSFC site. Indeed, measurement redundancy and instrument intercomparisons were key factors helping to increase the accuracy of aerosol absorption measurements.

3) Inferred values of the effective UV imaginary refractive index were first used for comparisons of aerosol single scattering albedo, *w*, at 325nm, 332nm and 368nm and with AERONET retrievals at 440nm, w_{440} [25]. The measured differences in absorption between 368nm and 440nm might

suggest the presence of selectively UV absorbing aerosols[5] or interference from gases other than ozone. However, the differences might also be caused by uncorrected systematic instrumental effects or absolute calibration uncertainties of sky radiances (~5% for almucantar technique[26]). Continuing co-located measurements at GFSC location is important to improve the comparison statistics, but conducting these measurements at different sites with varying background aerosol conditions is also desirable.

4) Using all cases for cloud-free days we derived the diurnal and seasonal dependence of aerosol absorption optical thickness, t_{abs} in the UV wavelengths. The expected accuracy of t_{abs} retrieval from UV-MFRSR measurements is ~0.01 to 0.02 limited by the UV-MFRSR measured accuracy and calibration (V_0). The variability in aerosol size distribution and real refractive index becomes comparable to the measured uncertainties only for large aerosol loadings (t_{ext}>0.5). The t_{abs} values show a pronounced seasonal dependence of t_{ext} with maximum values t_{abs} ~0.1 occurring in summer hazy conditions[5] and <0.02 in winter-fall seasons, when aerosol loadings are small.

5) It was found that ω decreases with decreases in t_{ext}. This could be due to real changes in the average aerosol composition between summer and winter month at the GSFC site. Obviously, continuation of UV-MFRSR measurements at the GSFC site with an enhanced unit (adding 440nm channel) is important to increase confidence in reported data.

In the future we suggest:

1) Providing spectral overlap measurements for shadowband and almucantar techniques. This involves: absolute calibration of UV sky radiance channels of CIMEL instruments (340nm and 380nm) and extending almucantar inversion techique[25-27] to include UV sky scans. For the shadowband technique replacing filters in one or several channels of UV-MFRSR instrument to match those of CIMEL instrument will be also helpful;
2) Adding spectrometer measurements to separate between aerosol and gaseous absorption;
3) Conducting measurements at different sites with larger expected UV aerosol absorption (more polluted sites with a higher black carbon fraction) or different types of aerosol (for sites with predominantly dust larger absorption is expected in UV than in the visible).

Acknowledgements

We thank members of USDA UVMRP and NASA AERONET projects for their support. We acknowledge NASA's Office of Earth Science (Code YS) for continued support through the TOMS Science Team and thank anonymous reviewer for suggesting substantial improvements to the paper.

REFERENCES

1. R. V. Martin, D.J.Jacob, R.N. Yantosca, M. Chin, P. Ginoux, "Global and regional decreases in tropospheric oxidants from photochemical effects of aerosols", *J. Geophys. Res. 108* (D3), 4097, doi:10.1029/2002JD002622, 2003.
2. S. He, and G.R. Carmichael, "Sensitivity of photolysis rates and ozone production in the troposphere to aerosol properties", *J. Geophys. Res***. 104,** 26307-26324, 1999.
3. H. Liao, Y.L. Yung, and J.H.Seinfeld, "Effects of aerosols on tropospheric photolysis rates in clear and cloudy atmospheres", *J. Geophys. Res***. 104,** 23697-23707, 1999.
4. M. Z. Jacobson, "Studying the effects of aerosols on vertical photolysis rate coefficient and temperature profiles over an urban airshed", *Journ. Geophys. Res.*, **103**, 10593-10604, 1998.
5. R.R. Dickerson, S. Kondragunta, G. stenchikov, K.L.Civerolo, B.G. Doddridge, and B.N.Holben, "The impact of aerosols on solar Ultraviolet radiation and photochemical smog", *Science* , 28, 827-830, 1997.
6. S. Madronich, *Environmental Effects of Ultraviolet (UV) Radiation*, chapter: UV radiation in the natural and perturbed atmosphere, *Lewis Publisher*, Boca Raton, 17-69, 1993.
7. N.A. Krotkov, P.K. Bhartia, J.R.Herman, V.Fioletov and J.Kerr, Satellite estimation of spectral surface UV irrdiance in the presence of tropospheric aerosols 1. Cloud-free case, *Journ. Geophys. Res*., 103, D8, 8779-8793, 1998.
8. J.R.Herman, N.Krotkov, E.Celarier, D.Larko, and G.Labow, "The distribution of UV radiation at the Earth's surface from TOMS measured UV-backscattered radiances," *J. Geophys. Res*., **104**, 12059-12076, 1999.
9. N.A. Krotkov, J.R.Herman, P.K. Bhartia, C. Seftor, Antti Arola, J. Kurola, S. Kalliscota, P. Taalas, I. Geogdzhaev, Version 2 TOMS UV algorithm: problems and enhancements, Opt. Eng. 41 (12) , 3028-3039, 2002.
10. N. A. Krotkov, J.R.Herman, P.K.Bhartia, C.Seftor, A.Arola, J.Kaurola, P.Taalas, I.Geogdzhaev, A. Vasilkov, OMI surface UV irradiance algorithm, P.Stammes (Ed.), vol. 3, ATBD-OMI_03, (http://eospso.gsfc.nasa.gov/eos_homepage/for_scientists/atbd/docs/OMI/ATBD-OMI-03.pdf).
11. V. E. Fioletov, J.B.Kerr, D.I.Wardle, N. Krotkov, J.R. Herman, "Comparison of Brewer ultraviolet irradiance measurements with total ozone mapping spectrometer satellite retrievals", *Opt. Eng*. **41** (12) 3051-3061, 2002.
12. J. B. Kerr, G.Seckmeyer, A.F.Bais, G. Bernhard, M.Blumthaler, S.B. Diaz, N.Krotkov, D.Lubin, R.L.McKenzie, A.A.Sabziparvar, and J.Verdebout, "Surface Ultraviolet Radiation:Past and Future", Chapter 5 *In Scientific Assesment of Ozone Depletion*: 2002, Global Ozone Research and Monitoring Project, *Report N 47, World Meteorological Organization, Geneva, 2003.*
13. V.E. Fioletov, M.G. Kimlin, N.A. Krotkov, L.J.B. McArthur, J.B.Kerr, D.I.Wardle, J.R.Herman, R. Metltzer, T.W. Mathews and J. Kaurola, UV index climatology over North America from ground-based and satellite estimates, accepted *J. Geophys. Res*., 109, D22308, doi:10.1029/2004JD004820, 2004

14. G.A. d'Almeida, P. Koepke, and E.P. Shettle, "Atmospheric aerosols: global climatology and radiative characteristics", A. Deepak Publ., Hampton, Vi., 557pp, 1991

15. I.N. Sokolik and O.B. Toon, Incorporation of mineralogical composition into models of the radiative properties of mineral aerosol from UV to IR wavelengths, *J. Geophys. Res.* , 104, (D8), 9423-9444, 1999.
16. S.C. Alfaro, S. Lafton, J.L.Rajot, P. Formenti, A. Gaudichet, and M.Maille, Iron oxides and light absorption by pure desert dust: An experimental study, *J. Geophys. Res., 109,* D08208, doi:10.1029/2003JD004374, 2004
17. J. T. Twitty and J. A. Weinman, "Radiative properties of carbonaceous aerosols", *J. Applied Meteorol*, 10, 725-731, 1975
18. H. Horvath, "Atmospheric light absorption – A review", *Atmos. Environ*, 27A, 293-317, 1993
19. J.D. Lindberg, R.E. Douglass, and D. M. Garvey, "Carbon and the optical properties of atmospheric dust", Applied Optics, 32 (30), 6077-6081, 1993
20. R. W. Bergstrom, P.B. Russell, and P. Hignett, "Wavelength Dependence of the Absorption of Black Carbon Particles: Predictions and Results from the TARFOX Experiment and Implications for the Aerosol Single Scattering Albedo", *J. Atm. Sci*., 59,567-577, 2002
21. R. W. Bergstrom, P.Pilewskie, B. Schmid, and P.B. Russel, "Estimates of the spectral aerosol single scattering albedo and aerosol radiative effects during SAFARI 2000", *J. Geophys. Res*, 108 (D13), 8474, doi:10.1029/2002JD002435, 2003

22. M. Z. Jacobson, "Isolating nitrated and aromatic aerosols and nitrated aromatic gases as sources of ultraviolet light absorption", *Journ. Geophys. Res.*, **104**, 3527-3542, 1999.
23. T. W. Kirchstetter, T. Novakov, P. Hobbs, "Evidence that the spectral dependence of light absorption by aerosols is affected by organic carbon", *J. Geophys. Res***. 109**, D21208, doi:10.1029/2004JD004999, 2004.
24. R. W. Bergstrom, et al., "Spectral absorption of solar radiation by aerosols during ACE-Asia, *J. Geophys. Res*, 198 (D19S15), 8474, doi:10.1029/2003JD004467, 2004

25. O. Dubovik and M.D. King, "A flexible inversion algorithm for retrieval of aerosol optical properties from Sun and sky radiance measurements", *J. Geophys. Res* ., **105**, D16, 20673-20696, 2000.
26. O. Dubovik, A. Smirnov, B.N. Holben, M. D. King, Y. J. Kaufman, T. F. Eck, and I. Slutsker, "Accuracy assessments of aerosol optical properties retrieved from Aerosol Robotic Network (AERONET) Sun and sky radiance measurements", *J Geophys. Res*., **105**, D8, 9791-9806, 2000.
27. O. Dubovik, B.Holben, T.Eck, A. Smirnov, Y. J. Kaufman, M. D. King, D. Tanre, and I. Slutsker, Variability of Absorption and Optical properties of key aerosol types observed in worldwide locations, *J. Atmos. Sciences*, **59**, 590-608, 2002.
28. T. F. Eck, B.N.Holben,J.R. Reid, et al., "High aerosol optical depth biomass burning events: A comparison of optical properties for different source regions" , Geophys. Res. Lett., 30 (20), 2035, doi: 10.1029/2003GL017861, 2003

29. B. M. Herman, S.R. Browning, J.J.DeLuisi, "Determination of the effective imaginary term of the complex refractive index of atmospheric dust by remote sensing: The diffuse-direct radiation method", *J. Atm. Sciences*, **32**, 918-925, 1975.

30. King, M. and B.M. Herman, "Determination of the ground albedo and the index of absorption of atmospheric particles by remote sensing. Part I: Theory", *J. Atmos. Sciences*, **36**, 163-173, 1979.
31. M. King, "Determination of the ground albedo and the index of absorption of atmospheric particles by remote sensing. Part II: Application", *J.Atmos. Sciences*, **36**, 1072-1083, 1979
32. T. F. Eck, B.N. Holben, I. Slutsker, and Alberto Setzer, "Measurements of irradiance attenuation and estimation of aerosol single scattering albedo for biomass burning aerosols in Amazonia*", J. Geophys. Res*., **103**, 31865-31878, 1998.
33. T. F. Eck, B. N. Holben, D. E. Ward, M. M. Mukelabai, O. Dubovik, A. Smirnov, J. S. Schafer, N. C. Hsu, S. J. Piketh, A. Queface, J. Le Roux, R. J. Swap, and I. Slutsker, "Variability of biomass burning aerosol optical characteristics in southern Africa during the SAFARI 2000 dry season campaign and a comparison of single scattering albedo estimates from radiometric measurements", J. Geophys. Res., 108(D13), 8477, doi:10.1029/2002JD002321, 2003.
34. T.A. Tarasova, I.A. Gorchakova, M.A. Sviridenkov, P.P.Anikin, and E.V.Romashova, "Estimation of the radiative forcing of smoke aerosol from radiation measurements at the Zvenigorod scientific station in the summer of 2002", Izvestiya, Atmospheric and Oceanic Physics, 40 (4) 454-463, 2004
35. B.N. Holben et al., "AERONET – A federated instrument network and data archive for aerosol characterization", *Remote Sensing Environment*, 66, 1-16, 1998.
36. B.N. Holben et al., "An emerging ground-based aerosol climatology: Aerosol Optical Depth from AERONET", *Journ. Geophys. Res.*, **106**, 12 067-12 097, 2001.
37. A. Kylling, A. F. Bais, M. Blumthaler, J. Schreder, C.S. Zerefos, and E. Kosmidis, "Effect of aerosols on solar UV irradiances during the Photochemical activity and solar ultraviolet radiation campaign", *Journ. Geophys. Res.*, **103**, 26051-26060, 1998.
38. B.N. Wenny, J. S. Schafer, J.J. DeLuisi, V.K. Saxena, W.F. Barnard, I. V. Petropavlovskikh, and A.J. Vergamini, "A study of regional aerosol radiative properties and effects on ultraviolet-B radiation, ", *Journ. Geophys. Res.*, 103 (D14), 17083-17097, 1998
39. J. Reuder and H. Schwander, "Aerosol effects on UV radiation in nonurban regions", *Journ. Geophys. Res.*, **104**, 4065-4077, 1999.
40. B. N. Wenny, V.K. Saxena, and J.E. Frederick, "Aerosol optical depth measurements and their impact on surface levels of ultraviolet-B radiation", *Journ. Geophys. Res.*, **106**, 17311-17319, 2001.
41. J.L.Petters, V.K. Saxena, J.R. Slusser, B.N. Wenny, and S. Madronich, "Aerosol single scattering albedo retrieved from measurements of surface UV irradiance and a radiative transfer model", *Journ. Geophys. Res*, 108 (D9) 4288, doi:10.1029/2002JD002360, 2003.
42. M.A.Wetzel, G.E. Shaw, J. R. Slusser, R.D. Borys, and C. F. Cahill, "Physical , chemical, and ultraviolet radiative characteristics of aerosol in central Alaska", *Journ. Geophys. Res*, 108 (D14) 4418, doi:10.1029/2002JD003208, 2003.

43. L. Harrison, J. Michalsky, and J. Berndt, "Automated Multi-Filter Rotating Shadowband Radiometer: An instrument for Optical Depth and Radiation Measurements", *Appl. Optics*, **33**, 5118-5125, 1994.

44. L. Harrison and J. Michalsky, "Objective algorithms for the retrieval of optical depths from ground-based measurements", *Appl. Optics*, **33**, 5126-5132, 1994.
45. D.S. Bigelov, J.R. Slusser, A. F. Beaubien, and J. R. Gibson, "The USDA ultraviolet radiation monitoring program", *Bull. Amer. Meteor. Soc.*, **79**, 601-615, 1998
46. N.A. Krotkov, P.K. Bhartia, J.R.Herman, J. Slusser, G. Scott, G. Jason, G. Labow, T. F. Eck and B. N. Holben, "UV aerosol absorption experiment (2002-04): 1. UV-MFRSR calibration and performance at GSFC", Opt. Eng., this issue, 2005
47. J. Slusser, et al., "Comparison of column ozone retrievals by use of an UV multifilter rotating shadow-band radiometer with those from Brewer and Dobson spectrophotometers", *Appl. Optics*, **38**, 1543-1551, 1999
48. W. Gao et al., "Direct-sun column ozone retrieval by the ultraviolet multifilter rotating shadow-band radiometer and comparison with those from Brewer and Dobson spectrophotometers", *Appl. Optics, 40*, 3149-3155, 2001
49 J. R. Slusser, J.H. Gibson, D. Kolinski, P. Disterhoft, K. Lantz, and A.F. Beabien, "Langley method of calibrating UV filter radiometer", *J. Geophys. Res.* , 105, 4841-4849, 2000.
50. Lantz, K., P. Disterhoft et al., "The 1997 North American Interagency Intercomparison of Ultraviolet Spectroradiometers Including Narrowband Filter Radiometers", *J. Res. Natl. Inst. Stand. Technology*, 107, 19-62, 2002.
51. J.A. Kaye, J.A., B.B. Hicks, E.C. Weatherhead, C.S. Long, and J.R. Slusser, "US Interagency UV Monitoring Program Established and Operating", *EOS*, 80 (10), 114-116, 1999
52. A. Smirnov, B.N.Holben, T.F.Eck, O.Dubovik, and I. Slutsker, "Cloud screening and quality control algorithms for the AERONET data base", *Rem. Sens. Env*., 73(3), 337-349, 2000
53. T.F. Eck, B.N.Holben, J.S.Reid, O.Dubovik, A.Smirnov, N.T.O'Neill, I.Slutsker, and S.Kinne, Wavelength dependence of the optical depth of biomass burning, urban and desert dust aerosols, *Journ. Geophys. Res.*, **104**, 31333-31350, 1999.
54. J.R. Herman and E. Celarier, "Earth surface reflectivity climatology at 340 to 380 nm from TOMS data," *J. Geophy. Res*., **102**, 28003-28011, 1997.
55. Herman, B. M., T. R. Caudill, D. E. Flittner, K. J. Thome, and A. Ben-David, A comparison of the Gauss-Seidel spherical polarized radiative transfer code with other radiative transfer codes, Appl. Opt, 34, 4563-4572, 1995.
56. K. Stamnes, et al., Numerically stable algorithm for descrete-ordinate-method radiative transfer in multiple scattering and emitting layered media, *Appl. Opt., 27*, 2502-2509, 1988.
57. R. Kotchenruther, R., and P.V. Hobbs, "Humidification factors of aerosols from biomass burning in Brazil", *J. Geophys. Res*., 103, 32,081-32090, 1998.
58. J. A., Jr., Coakley , and P.Chylek, "The two-stream approximation in radiative transfer: Including the angle of the incident radiation", *J. Atmos. Sci*., 32,409-418, 1975
59. Arola et al, "Assessment of TOMS UV bias due to absorbing aerosols", UV Ground and Space-based measurements , Models and Effects IV, edited by James R. slusser , Jay R. Herman, wei Gaom Germar Bernhard, Prpceedings of SPIE, V. 5545, pp. 28-35,2004.

Appendix 1: SENSITIVITY OF UV-MFRSR MEASUREMENTS TO AEROSOL ABSORPTION

Standard UV-MFRSR measurements include voltages that are proportional to total horizontal and diffuse horizontal irradiance components. Since both components are measured by the same diffuser/filter/detector combination, diffuse and total atmospheric transmittances are obtained directly from the measured voltage ratios: $T_D = V_D/V_0$ and $T_T = V_T/V_0$. Here V_0 is extraterrestrial voltage obtained by calibration transfer from AERONET network sun-photometers[18,19] as previously described[38]. The diffuse and total transmittances are not independent, since the voltage difference (V_T - V_D) has been used for the direct-sun equivalent calibration V_o, and to infer aerosol extinction optical thickness, t_{ext},. Therefore, only one additional aerosol parameter could be independently estimated in each UV-MFRSR spectral channel by matching transmittances for each wavelength (or their ratios) to those calculated from a radiative transfer model. Our goal is to infer aerosol absorption optical thickness, t_{abs}, while other model input parameters are constrained by independent measurements. We note that UV surface albedo is low and stable at our site for snow free conditions (~0.02-0.03 from clear-sky overpass EP/TOMS reflectivity measurements), and does not have a noticeable effect on ground based aerosol measurements.

Historically, different irradiance ratios were used to infer t_{abs} (or aerosol single scattering albedo, $\omega=1-\tau_{abs}/\tau_{ext}$): diffuse/direct ratio, $DD=T_D/(T_T-T_D)$[13, 20-22], diffuse fraction (diffuse/total, $DT=T_D/T_T$) ratio[23,24] and total to Rayleigh transmittance ratio ($TR=T_T/T_{Ray}$)[6]. In the end, all inversion techniques should deliver consistent t_{abs} retrieval results regardless of which input data are used. For our measurements of t_{abs}, the most convenient quantity is the total (T_T =*direct plus diffuse*) atmospheric transmittance, which is directly related to aerosol absorption and is least sensitive to aerosol size distribution and extinction optical thickness, t_{ext}. In the UV spectral region, where t_{Rayleigh} typically exceeds that of t_{aerosol}, it is convenient to normalize T_T by total transmittance of the molecular atmosphere with the same ozone amount, $TR=T_T/T_{Ray}$, which greatly reduces sensitivity to ozone, wavelength and solar zenith angle. An important advantage of working with TR is that non-absorbing aerosols have only a small effect on *TR* (τ~0.1 produces ~1% *TR* reduction)[6], since the decrease in direct solar flux caused by aerosol scattering is nearly compensated by an increase in diffuse sky flux. For UV absorbing aerosols (*dust, smoke* and *urban*), the increase in the diffuse flux is suppressed by aerosol absorption, so *TR* sensitivity to t_{abs} is an order of magnitude greater than *TR* sensitivity to t_{ext}. Based on a modeling study[6] the dependence of *TR* on t_{ext} and t_{abs} can be written approximately as:

$$-\ln(TR) \approx a t_{ext} + b t_{abs} \qquad \text{(a1)}$$

where, for typical aerosols (not containing significant quantities of mineral dust and smoke), a~0.1 and b~2-3 (increasing with solar zenith angle). To better estimate a and b *TR* and t_{abs} were re-calculated for fixed values of solar zenith angle, q_o and t_{ext} using AERONET individual almucantar inversions at GSFC in 2002-2003[25-27].

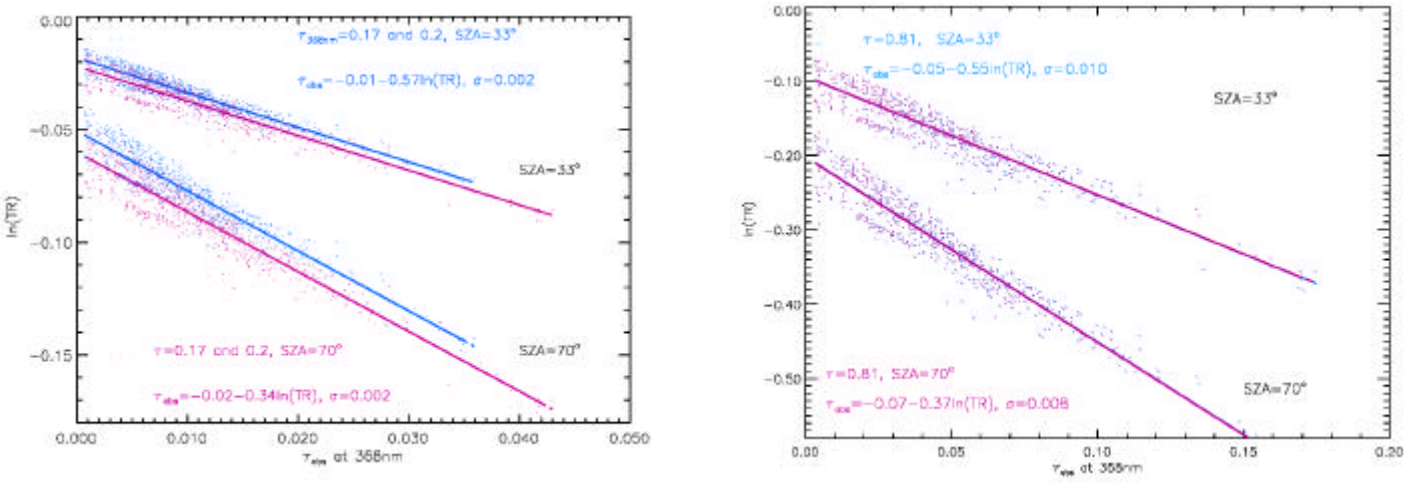

Figure A1 Relationship between Rayleigh normalized total transmittance, TR and t_{abs} at 368nm, assuming fixed t_{ext}=0.167 (red) and 0.2 (purple) and q_o=33°,70°. Linear regression model (1) is fitted to al data points assuming variability due to size distribution as random errors

The linear regression model, equation (A1), was fitted to all calculated pairs (T_R, t_{abs}) to estimate T_R sensitivity selectively to t_{abs}, treating real variability in size distribution and real part of refractive index, n_R, as random errors (Figure A1).

The regression coefficients quantify *TR* sensitivity to aerosol parameters as function of solar zenith angle (Table A1). The expected accuracy of t_{abs} retrieval from UV-MFRSR measurements is ~0.008-0.02 limited by the measured accuracy of total voltage (V_T) and calibration (V_0)[46]. The variability in aerosol size distribution and real refractive index becomes comparable to the measured uncertainties only for large aerosol loadings (t_{ext}>0.5). The measurement uncertainties (discussed in detail in the first paper[46]) and regression coefficients for high and low aerosol loadings are summarized in Table A1. The estimated retrieval uncertainties of t_{abs} and ω for shadowband technique (Table A1) are comparable to almucantar technique[25-27] for favorable conditions (large solar zenith angles, q_o >45° and high aerosol loadings t_{ext}(440nm)>0.4). However, an important advantage of the shadowband technique is that it remains sensitive to t_{abs} even at low solar zenith angles, when the almucantar technique is not sensitive to t_{abs}.[25-27] On the other hand, cosine correction errors increase for shadowband measurements at high solar zenith angles (see discussion in the first part), while cosine errors are absent for the CIMEL. Thus, the two types of measurements are required for measuring complete diurnal cycle of aerosol absorption.

Figure captions

Figure 1 UV-MFRSR and AERONET single scattering albedo retrieval at GSFC on June 2 2003. The 3-minute UV-MFRSR retrieved single scattered albedos at 368nm are shown as small purple spheres, while AERONET ω_{440} retrievals at 440nm are shown as large crosses with +/- 0.03 error bars[26]. The actual solar zenith angle was used in retrieval for each 3-min UV-MFRSR measurement. The UV-MFRSR assumptions were: surface albedo 0.02, Brewer measured total ozone, boundary layer aerosol profile and Dubovik and King[25]inverted particle size distribution within +/- 30min of each CIMEL almucantar measurement.

Figure 2 UV-MFRSR and AERONET ω retrieval at GSFC on June 24, 2003. The 3-minute UV-MFRSR ω_{368} is shown as small purple spheres, while AERONET ω_{440} retrievals are shown as large crosses with ±0.03 error bars[27]. In addition, τ_{ext} at 368nm is shown for both instruments (same symbols) with right axis scale. The actual solar zenith angle was used in retrieval for each 3-min UV-MFRSR measurement. The UV-MFRSR assumptions were: A= 0.02, Brewer measured total ozone, boundary layer aerosol profile and AERONET [25]inverted particle size distribution within ±30min of each CIMEL almucantar measurement.

Figure 3. UV-MFRSR and AERONET ω retrieval at GSFC on August 25, 2003. The 3-minute UV-MFRSR ω_{368} is shown as small purple spheres, while AERONET ω_{440} retrievals are shown as large crosses with ±0.03 error bars[27]. In addition, τ_{ext} at 368nm is shown for both instruments (same symbols) with right axis scale. The actual solar zenith angle was used in retrieval for each 3-min UV-MFRSR measurement. The UV-MFRSR assumptions were: surface albedo 0.02, Brewer measured total ozone, boundary layer aerosol profile and AERONET [25]inverted particle size distribution within ±30min of each CIMEL almucantar measurement.

Figure 4. Timeseries of aerosol absorption optical thickness τ_{abs} at 368nm, derived from 17 months UV-MFRSR operation at NASA GSFC site in Maryland, US. The data are for cloud-free and snow free conditions. Individual $\tau_{abs}(368)$ values were averaged over 1-hour period of time within ±30min of the AERONET inversion. The error bars of $\tau_{abs}(368)$ are interpolated by $\tau_{abs}(368)$ and solar zenith angle from estimates given in Appendix Table A1

Figure 5. Hourly average retrieved values $<\omega_{368}>$ as function of measured extinction optical thickness, τ_{abs} at 368nm for 17 months UV-MFRSR operation at NASA GSFC site in Maryland, US. The error bars are interpolated from Table A1 (Appendix) and are the same as for individual retrievals. The error bars were not reduced, despite 1 hour averaging of individual retrievals, because retrieval errors were not believed to be random. Only $<\omega_{368}>$

Figure 6 The ratio between satellite estimated (by TOMS UV algorithm[7-10]) and measured (by UV-MFRSR) total (direct plus diffuse) surface UV irradiance at 325nm versus aerosol absorption optical thickness at 325nm inferred from combined UV-MFRSR and AERONET measurements at NASA GSFC site. The line shows theoretical relationship derived from radiative transfer modeling[10]. The results are shown only for pollution aerosols with TOMS absorbing aerosol index, AI at 331nm less than 0.5 and TOMS 360nm Lambertian effective reflectivity

Appendix

Figure A1 Relationship between Rayleigh normalized total transmittance, TR and τ_{abs} at 368nm, assuming fixed solar zenith angle θ_o=33^o,70^o and extinction optical thickness τ_{ext} (a) 0.167 (red) and 0.2 (purple) (b) τ_{ext}=0.8(red) τ_{ext}=0.82 (purple). Linear regression model (1) is fitted to al data points assuming variability due to size distribution as random error. Regression coefficients are given in Table 1.

Table A1 UV-MFRSR measurement errors, sensitivity to t_{abs} for different conditions and expected retrieval errors

Sources of measured errors in UV-MFRSR 368nm channel	τ=0.2		τ=0.8	
	θ=33	θ=70	θ=33	θ=70
	Daily V_0 calibration error, $s_{\ln V_0}$			
ΔlnV0 (V0~2100mv) [1] $s_{\ln V_0}$	0. 01 (0.05)	0. 01 (0.05)	0. 02 (0.1)	0.02 (0.1)
	Combined *TR* measurement and calibration errors			
Combined *TR* measurement error: $s_{\ln(TR)}$ 2)	~0.022 (0.05)	~0.022 (0.05)	~0.036 (0.1)	~0.036 (0.1)
	Measurement sensitivity: $\frac{\partial \ln(V_T)}{\partial(t_y)}$			
Sensitivity ln(VT/V0) to τ_{abs}	1.8	2.9	1.8	2.7
Sensitivity ln(VT/V0) to τ_{ext}	0.1	0.17	0.1	0.17
	Expected retrieval errors			
Expected error in τ_{abs} due to measurement error, 1σ	0.01 (0.03)	0.007 (0.02)	0.02 (0.05)	0.013 (0.05)
Expected error in τ_{abs} due to uncertainty in PSD, 1σ [3]	0.006	0.003	0.01	0.01
Combined error in $\tau_{abs,}$ 1σ	0.012 (0.03)	0.008 (0.02)	0.022 (0.051)	0.016 (0.05)
Error in ω~ $\frac{\Delta t_{abs}}{t_{ext}}$ [4]	0.06 (0.15)	0.04 (0.10)	0.03 (0.06)	0.02 (0.06)

1) AERONET V_o uncertainty for reference instruments combined with calibration transfer error (see part1 paper); 2) Assuming that calibration and *VT* measurement errors are uncorrelated (see part 1 paper [46]); (3) The scatter of points around regression line (equation A1 in Appendix) gives estimate of the retrieval noise if size distribution information is not used in τ_{abs} retrieval; (4) Using relationship $\omega=1-\tau_{abs}/\tau_{ext}$, assuming constant error in $\tau_{ext:}$ $\sigma_{\tau ext}$~0.01 and uncorrelated errors in errors in τ_{ext} and τ_{abs}.

Table 1 Summer (2003) aerosol single scattering albedo statistics[1)]

Parameter		UV-MFRSR[2)]			AERONET[3)]	
		325nm	332nm	368nm	440nm	670nm
Mean single scattering albedo, ω	$<\omega>$ (ω_{min} : ω_{max})	0.92 (0.86:0.95)	0.92 (0.86:0.95)	0.94 (0.89:0.97)	0.96 (0.91 :0.99)	0.95 (0.88 :0.99)
Standard deviation, ω	σ_ω	0.025	0.024	0.02	0.017	0.021
Mean ω difference	$<\Delta\omega_\lambda>=$ $<\omega_{440} - \omega_\lambda>$	0.04 (0.0 : 0.09)	0.04 (0.0 : 0.09)	0.02 (0.0:0.06)	0	0.007 (0.0:0.03)
Standard deviation of $\Delta\omega_\lambda$	$\sigma_{\Delta\omega\lambda}$	0.02	0.019	0.015	0	0.01
Correlation coefficient ω_λ with ω_{440}	$R(\omega_\lambda,\omega_{440})$	0.61	0.61	0.67	1	0.95
Correlation coefficient ω_λ with ω_{368}	$R(\omega_\lambda,\omega_{368})$	0.92	0.92	1	0.67	0.59

1) *Data sample (N=60) with solar zenith angle between 45^o and 70^o, t_{440}> 0.4 was predominantly for summer 2003*
2) *Sample included 2 hour averaged UV-MFRSR w retrievals (between 10 and 40 individual retrievals)*
3) *Sample included individual AERONET w inversions*

Table 2 Summer (2003) Imaginary refractive index statistics.[1)]

Parameter		UV-MFRSR[2)]			AERONET[3)]	
		325nm	332nm	368nm	440nm	670nm
Mean absorption index, 10^3k	$10^3\langle k\rangle$ 10^3 (k_{min} : k_{max})	13 (7 : 27)	13 (7 : 26)	9 (5 : 20)	6 (0.8 : 13)	5 (0.8 : 12)
Standard deviation, k	$10^3\sigma_k$	5	5	4	3	2.82
Mean k difference: $10^3\Delta k_\lambda$	$10^3\langle k_\lambda - k_{440}\rangle$	7.6 (0 : 20)	7 (0 : 19)	3.6 (-1 : 12)	0	0.3 (-1 : 1)
Standard deviation of the k difference	$10^3\sigma_{\Delta k\lambda}$	3.7	3.6	2.5	0	0.4
Correlation coefficient k_λ with k_{440}	$R(k_\lambda,k_{440})$	0.69	0.68	0.75	1	0.99
Correlation coefficient k_λ with k_{368}	$R(k_\lambda,k_{4368})$	0.95	0.95	1	0.75	0.73

1) *Sample (N=60) for solar zenith angle between 45 and 70^o, and t_{440}> 0.4 predominantly for summer 2003*
2) *Sample included 2 hour averaged UV-MFRSR k retrievals (10 – 30 individual retrievals)*
3) *Sample included individual AERONET k inversions*

Table 3 Annual (2002-2004) aerosol absorption optical thickness t_{abs} statistics.

Parameter		UV-MFRSR[2)]			AERONET[3)]	
		325nm	332nm	368nm	440nm	670nm
Mean τ_{abs}	$<\tau_{abs}>$ $(_{min} : _{max})$	0.05 (0.007 : 0.12)	0.05 (0.009 : 0.11)	0.04 (0.007 : 0.09)	0.02 (0.003 : 0.05)	0.01 (0.001 : 0.03)
Standard deviation, τ_{abs}	$\sigma_{\tau abs}$	0.02	0.02	0.015	0.01	0.007
Mean τ_{abs} difference	$\Delta\tau_{abs}(\lambda) = <\tau_{abs}(\lambda) - \tau_{abs}(440)>$	0.03 (- 0.001 : 0.08)	0.03 (- 0.001 : 0.07)	0.02 (- 0.01 : 0.05)	0	-0.01 (-0.03 : -0.002)
Standard deviation of the difference $\Delta\tau_{abs}(\lambda)$	$\sigma_{\Delta\tau abs}$	0.014	0.013	0.01	0	0.005
Correlation coefficient $\tau_{abs}(\lambda)$ with $\tau_{abs}(440)$	$R(\tau_{abs}(440),\tau_{abs}(\lambda))$	0.84	0.81	0.76	1	0.98
Correlation coefficient $\tau_{abs}(\lambda)$ with $\tau_{abs}(368)$	$R(\tau_{abs}(368),\tau_{abs}(\lambda))$	0.93	0.95	1	0.76	0.74

1) *Data sample (N=260) with solar zenith angle between 20^o and 70^o, and $t_{440} > 0.1$ in 2002- 2004.*
2) *Sample included 2 hour averaged UV-MFRSR k retrievals (between 10 and 40 individual retrievals)*
3) *Sample included individual AERONET k inversions*